

Joint Potential-Vector Fields for Obstacle-Aware Legible Motion Planning

Huy Quyen Ngo¹ and Aaron Steinfeld¹

Abstract—Traditionally, potential fields and vector fields have been extensively used for motion planning, especially in finding paths to a goal position while avoiding obstacles along the way. However, such methods have only been applied to the problem of finding the shortest path to only one goal position. In human-centered environments with multiple goals, the shortest path (e.g., most predictable) is often not the most intent-expressive path (e.g., most legible) to one of the goals. We devised a method for robot planning and navigation in human-centered environments that uses potential fields to plan intent-expressive motion to a specific goal among many, while utilizing adaptive vector fields to avoid obstacles without sacrificing the legibility property of the motion. We found that our method can produce motions that are of comparable legibility and shorter path length compared to a legible motion planner baseline, as well as more legible paths compared to a traditional potential field method. Our method was evaluated in several scenarios where legibility is useful, namely maps with and without obstacles and goal switching.

I. INTRODUCTION

Motion planning has been a major active research areas in robotics, with applications spanning diverse uses from mobile robot servers in restaurants [1], robotic manipulators handing over objects to humans [2], cars driving in the road [3], and UAVs in the sky [4]. Motion planning, coupled with obstacle avoidance, ensures a safe path from a starting position to a goal position, without creating harmful interactions on the way. Moreover, in human-centered environments, communicating intention in complex situations (i.e., having multiple available goals) requires special planning efforts, as the shortest path is the most predictable but not always intent-expressive [5]. Thus, being able to generate legible motions in complicated environments, in which multiple goals and possible obstacles are present, is extremely important in providing safety and intent-expressiveness in robot behaviors in human-centered environments.

We drew inspiration from established motion planning methods, namely Potential Field (PF) [6] and Vector Field (VF) [7] planning methods, to devise a new technique for the generation of obstacle-aware legible motions. Traditionally, PF utilizes a physics-based model of attractive and repulsive forces acting on the agent, where the agent is constantly pulled towards the goal and pushed away from obstacles. In scenarios having more than one available goal positions, the real goal attracts the agent and the other goals repel it,

*This work was supported by the Office of Naval Research award N00014-18-1-2503.

¹Huy Quyen Ngo and Aaron Steinfeld, Robotics Institute, Carnegie Mellon University, Pittsburgh, Pennsylvania, USA
huyquyen@andrew.cmu.edu, steinfeld@cmu.edu

expressing the intention of going to that real goal and not others. On the other hand, VF creates circular force fields around obstacles, making the agent diverge its path when traveling near the obstacles. In our method, the agent can determine the direction of the circular force field of any nearby obstacle based on the relative position of the goal and the obstacle about the current heading direction of the agent. Combining the attracting and repelling effects of the real goal and other goals with the adaptive circular force fields of nearby obstacles produces a generalized legible motion planner with obstacle avoidance that can be applied to arbitrary goals and obstacles with different sizes, effective radii, and force scaling parameters. Such generated motions are not only intent-expressive towards one of the available goals, but also safe as they avoid obstacles on the way from the starting position to the goal. Previous legible motion planning work has not focused on this obstacle avoidance capability (e.g., [8]).

We applied our method in a few cases where legibility is highly relevant. The first case was similar to the scenario in Taylor et al. [1], where a robot server delivers food to one of two tables in a restaurant. The second case was similar to the first case, but with obstacles on the original planned path to the restaurant table, which can be another robot server, a human customer, or simply a newly popup table. Finally, the last case was inspired by the scenario of robot-to-human object handover (e.g., [9], [10], [11]), where the robot arm has to deliver an object to either the right or left hand of a human, and re-planning is necessary if the target hand is occupied. All those cases were modeled in a 2-dimensional map with an omniscient observer and a point robot navigating to one of the goals. In this paper, we simplified the obstacles as appearing on the map, rather than moving into the scene with arbitrary velocities and heading directions. We defer the case of legible planning with moving obstacles to a future work.

In summary, our contributions in this paper are listed as below:

- 1) An algorithm for determining the direction of circular vector force field of obstacles based on the relative goal and obstacle positions about the agent's current heading direction; and
- 2) An obstacle-aware legible motion planner that works on goals and obstacles with various sizes and tunable effective radii, force scaling parameters, and vector field strength.

II. RELATED WORK

A. Legible Motion Planning

Dragan et al. [12] pioneered the research on legible motion planning, in the context of expressing the robot's intent to go to one of many goals by exaggerating the motion. By imposing a trust region in which motions become arbitrarily unpredictable when outside of the region, the method was able to generate paths that are intent-expressive, but less predictable as predictability and legibility are contradictory properties of motion [5]. In a later work, Holladay et al. [13] constructed a planner focusing on pointing gesture to reference objects in cluttered environments with multiple objects. Using a ray-casting model, their method could generate pointing configurations that make the goal object as clear as possible. Although the observer's viewpoint plays a crucial role in the process, the method was able to trade off efficiency for clarity of the pointing.

Recognizing the importance of observer's viewpoint on legibility, Taylor et al. [1] developed a method for generating legible robot motions that indicate the robot's goal while in view of an observer. Verified by a 300-person online study on first-person videos in restaurant with a robot server scenario, their method was proven to be effective in the situation of two tables as goals, in which the robot server was delivering to one of the tables. While their planner could generate legible robot paths to the goal, it did not consider the situation where there were obstacles on the robot's path, which is the scenario we investigate here. In addition, Nikolaidis et al. [8] developed a legible planner that takes into account observer's viewpoint, with additional consideration of the occluded region in the map.

Choices in motion design can influence the collaboration performance in human-robot interaction. Particularly, robot arm motion can express intention to humans in collaborative tasks, such as placing a plate where humans thought the robot was going to place a cylinder [14]. Moreover, robots' hesitant gesture such as backward movement could also signal intention in facilitating order of passage and yield priority, with varying back-off length and speed [15].

B. Potential Field and Vector Field Motion Planning

The potential Field planning method was established to be effective for shortest path finding in the presence of obstacles [6]. Taking inspiration from physics-based model of attractive-repulsive forces, robots can avoid obstacles and travel to the goal by following the path with lowest potential function values. However, potential field generated paths can suffer from the local minimum point problem, in which the attractive-repulsive forces are balanced far from the actual goal. Sun et al. [16] solved this problem by adding a term of relative distance between the target and the robot in the repulsive potential field function, which ensured the target always being the global minimum potential. Although being effective in avoiding local minima, this method can still suffer from discontinuous paths where the instantaneous heading direction change of the robot is relatively large.

Alongside potential field planning, researchers have developed planners for motion planning and collision avoidance using vector fields, which can potentially resolve the problem of large instantaneous heading direction change of robots. Panagou [7] used vector fields to navigate the robot to the goal by following the circular forces around static obstacles, while the robot was under the attraction force of the goal. However, the method worked under the assumption that all the obstacles' force directions are fixed based on the position of the goal.

Wilhelm et al. [17] also attempted to solve the large instantaneous heading direction change by using a vector field for decreasing deviation from the original designated paths around obstacles. The method employed gradient vector field for path following and obstacle avoidance, which consists of weighted convergence and circulation components to generate guidance vectors toward and then along the path around the obstacle. In addition, Chen et al. [18] developed tangent vector filed guidance and Lyapunov vector field guidance for finding the shortest path under constraints of the UAVs.

While potential field planning methods and vector field planning methods are effective in obstacle-aware shortest path finding, they have not been applied to the problem of legible motion planning in the context of expressing intent to one of multiple goals. Our work drew inspirations from these methods to address the problem of legible motion planning [5] with obstacle avoidance.

C. Other Obstacle-Aware Planning Methods

Apart from potential fields [6], [19] and vector fields [7], other planning methods have been proven to work for obstacles in the map. Heuristic algorithms such as A* [20] and Dijkstra [21] represent the map as nodes with edges connecting them together, in which the edges have costs when traversing through them. In such cases, obstacles could be modeled as nodes such that the edges to them have very large cost, thus making the path avoiding those edges and the obstacles. Such methods inspired many later path planners which make the cost traveling to or near obstacles very large for obstacle avoidance. Other heuristic algorithms can update the heuristic estimate of the current state such as [22], as well as combining heuristic and incremental search to find paths in dynamic environment [23].

The strategy of finding an obstacle-aware path depending on the relative position of the goal and the start was considered in the family of BUG algorithms [24], [25]. These algorithms can find the shortest path to the goal, and the path finding strategy based on the relative position between the goal and the current robot position was an inspiration when developing our directional vector field for obstacle avoidance.

Finally, researchers have investigated obstacle avoidance during path planning with sampling-based method, such as Rapidly-Exploring Random Trees (RRT) [26], [27] and Probabilistic Roadmaps (PRMs) [28]. While those methods are well-established, they only work for known maps with known obstacles, thus discarding the real-time characteristics

of the system, in which our method focused on developing in this work.

III. METHOD

Our method combined the attractive-repulsive mechanism of Potential Field (PF) for the real goal and other goals with the directional circular Vector Field (VF) of nearby obstacles for legible obstacle avoidance.

A. Potential Field for Goals

In traditional PF, the global goal always attracts and the obstacles repel, creating a combined effect of pulling the agent to the goal and pushing the agent away from the obstacles. Inspired by those principles, we modeled the real goal of our situation having the attractive force and the other goals having the repulsive forces.

The attractive potential field functions of the real goal and the other goal can be represented as below:

$$U_{total} = U_{goal} + \sum_{other=1}^{N_{other}} U_{other} \quad (1)$$

$$U_{goal} = \frac{1}{2} k_p (d_{goal})^2 \quad (2)$$

$$U_{other} = \begin{cases} \frac{1}{2} k_n \left(\frac{1}{d_{other}} - \frac{1}{s_{other}} \right)^2, & d_{other} \leq s_{other} \\ 0, & d_{other} > s_{other} \end{cases} \quad (3)$$

where d_{goal} and d_{other} are the distance from the goal and the other goal to the agent, respectively; k_p and k_n are the gain coefficients of the attractive and repulsive forces, respectively; s_{other} is the maximum distance of influence for the repulsive force of the other goal (in our case, it is the distance between the starting position and the other goal location); and N_{other} is the number of other goals.

The attractive force and repulsive force functions are the negative gradient of the gravitational potential field functions of the goal and the other goal. To account for the problem of local minimum point of PF, we used the optimized repulsive force function in [16] to ensure that the real goal is always the global minimum point of the entire field. Specifically, we added a decaying term $(d_{goal})^n$ in the repulsive force function of the other goal, with n is the decay coefficient:

$$F_{total} = F_{goal} + \sum_{other=1}^{N_{other}} F_{other} \quad (4)$$

$$F_{goal} = -k_p d_{goal} \quad (5)$$

$$F_{other} = \begin{cases} k_n \left(\frac{1}{d_{other}} - \frac{1}{s_{other}} \right) \frac{(d_{goal})^n}{(d_{other})^2}, & d_{other} \leq s_{other} \\ 0, & d_{other} > s_{other} \end{cases} \quad (6)$$

By modeling the potential field as above, the agent always travels towards the real goal while steering clear of the other goals. This principle reflects the idea in legible motion planning [5], as the agent communicates the intention of the real goal being the target through the planned motion.

B. Vector Field for Obstacle Avoidance

We used directional VF for obstacle avoidance, in which its direction depends on the agent's heading when it first travels in the obstacle vector field's effective region. An example of an obstacle vector field is shown in Figure 1.

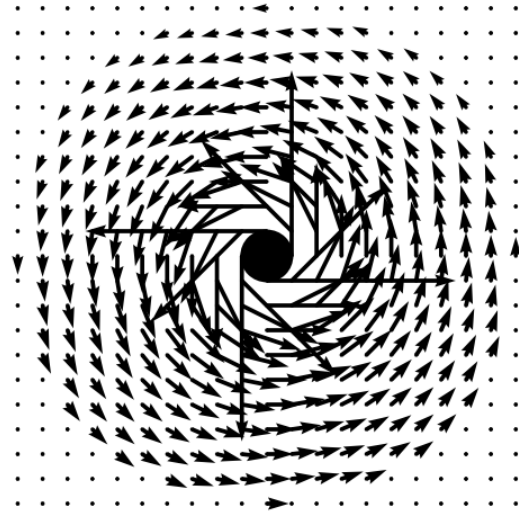


Fig. 1. Example obstacle with circular vector field. The field has a counterclockwise direction. The field strength is inversely proportional to the distance to the center of the obstacle (e.g., the closer to the center, the larger the force).

Our vector field for obstacles is modeled as below, with F_{ox} and F_{oy} being the vector forces in x and y directions:

$$F_{ox} = direction_f k_f \left(-\frac{p_y - o_y}{d_o^2} \right) (d_{goal})^m \quad (7)$$

$$F_{oy} = direction_f k_f \frac{p_x - o_x}{d_o^2} (d_{goal})^m \quad (8)$$

where p_x , p_y , o_x , and o_y are the x and y positions of the agent and the obstacle, respectively; d_o and d_{goal} are the distance from the obstacle and the goal to the agent; and k_f is the vector field strength coefficient; $direction_f$ is the circular direction of the vector field (1 for counterclockwise and -1 for clockwise). Finally, similar to Equation 6, the term $(d_{goal})^m$ is to ensure the real goal being the global minimum point for the entire field, with m is the decay coefficient. For this, m and n can have different values.

In order to determine the direction of the circular vector fields around obstacles, we imposed a check on the relative positions of the goal and the obstacle about the current heading of the agent when it first travels in the effective range of the obstacle vector field. This is partially inspired by the family of BUG algorithms [24], where the path planning process is based on the line between the start and the goal. If the goal and the obstacle are on opposite sides of the agent's heading, the obstacle vector field has a clockwise direction, and vice versa. The algorithm is shown in Algorithm 1. The $sign(Heading(Goal))$ is to account for different cases regarding relative positions of the two goals, which can

Algorithm 1 Obstacle Vector Field Direction

Require: *Agent, Heading, Obstacle, Range, Goal*

```

if Distance(Agent, Obstacle) <= Range then
    if Heading(Obstacle) * Heading(Goal) <= 0 then
        if Opposite Sides of the Heading Line
            Direction = -1                                ▷ Clockwise
        else
            Direction = 1                                ▷ Counterclockwise
        end if
    end if
Return sign(Heading(Goal)) * Direction

```

be calculated by plugging the position of the goal in the *Heading* line equation and take the sign of the result.

Compared to traditional potential field obstacle avoidance, where the repulsive force points directly outward from the center of the obstacle, this vector field allows smoother motion when avoiding the obstacle.

IV. EVALUATION METRICS

Our goal was to confirm that our method can generate paths that are more efficient than and of comparable legibility as [12], and more legible than [6]. The two metrics we used allow comparison of the legibility and efficiency of the paths: Area Under the Legibility Curve (AULC) and Total Path Length (TPL).

A. Area Under the Legibility Curve (AULC)

Inspired by Area Under The Curve (AUC) by Myerson et al. [29], AULC represents the legibility scores of the real goal over time, calculated by computing the AUC of the real goal's legibility scores. Due to our method not being an optimization approach, using only the final path's legibility score would potentially neglect the legibility of the earlier portions of the path. We used AULC for a comprehensive evaluation of the whole path's legibility.

To calculate the legibility score of a given path $\xi_{S \rightarrow \xi(t)}$, we used the formula in Dragan et al. [12] as below:

$$\text{legibility}(\xi) = \frac{\int P(G^* | \xi_{S \rightarrow \xi(t)}) f(t) dt}{\int f(t) dt} \quad (9)$$

in which $P(G | \xi_{S \rightarrow \xi(t)})$ is the probability of inferring goal G via path ξ from the start point S to an arbitrary point $\xi(t)$ on the path. Here, $\xi_{\xi(t) \rightarrow G}^*$ is the optimal path from the point $\xi(t)$ to goal G , and $\xi_{S \rightarrow G}^*$ is the optimal path from the start S to the goal G , which are straight paths. The probability $P(G | \xi_{S \rightarrow \xi(t)})$ is expressed as below:

$$P(G | \xi_{S \rightarrow \xi(t)}) \propto \frac{\exp(-C(\xi_{S \rightarrow \xi(t)}) - C(\xi_{\xi(t) \rightarrow G}^*))}{\exp(-C(\xi_{S \rightarrow G}^*))} P(G) \quad (10)$$

The cost function C was calculated by the sum squared velocities of the path:

$$C[\xi] = \frac{1}{2} \int \xi'(t)^2 dt. \quad (11)$$

We denote $\text{legibility}_G(\xi)$ is the legibility score of path ξ inferring goal G . Thus, the AULC of path ξ is:

$$\text{AULC}(\xi) = \text{AUC}(\text{legibility}_{\text{RealGoal}}(\xi)) \quad (12)$$

With this Area Under the Legibility Curve metric, we can conclude which path is more legible by comparing the magnitude of AULC. A more legible path has a larger AULC value, and vice versa.

B. Total Path Length (TPL)

The shortest path to a goal is a traditional path planning evaluation metric, motivating selection here. In this paper, TPL was computed as the sum of the lengths of all segments in the path, in which path with shorter length is considered more efficient:

$$\text{TPL}(\xi_{S \rightarrow G}) = \int_0^T \xi(t) dt. \quad (13)$$

in which ξ is the path, and T is the total time step to reach the goal G from the start point S .

To evaluate our method, we compared paths generated by our method, paths generated by traditional potential field method [6], and legible baseline paths generated by Dragan et al. [5] with our two metrics mentioned above, namely Area Under the Legibility Curve (AULC) and Total Path Length (TPL). For each case, the legibility scores over time of our method and baselines are described in Figure 5, and the total path length of each method is shown in Figure 6 in the last subsection of Results.

V. RESULTS

A. Simulation Settings

As mentioned earlier, our three evaluation cases were inspired by human-centered scenarios in which legibility is needed, namely robot servers in restaurant settings [1], [30] and robot-to-human object handover [9], [10], [11]. In the first case of no obstacle, the robot server has to deliver food to one of the two tables, in which legibility is necessary for expressing early intention of delivering food to the target table. The second case was similar to the first case in a restaurant setting, except having obstacles appear on the path. Those obstacles can be other robot servers, human customers, and newly popup tables in the restaurant, in which the robot server should navigate to avoid without sacrificing the legibility of the path. The final case highlighted the necessity of legible paths in a robot-to-human handover task, in which the robot arm should deliver an object to either the left or right hand of humans. At an arbitrary point, the robot realizes the target hand is occupied, thus re-planning an alternative path to the other hand expressing the intention change. All of these scenarios need legibility in robot motions, and were analyzed individually in this section.

We simulated our method on 2-dimensional map with Python and Matplotlib. Our parameters are listed in Table I for future reproduction of our results. Note that the other goal's effective range is the Euclidean distance between the

Other Goal and the Start position, thus having an odd value in the Parameter Table. The parameters can be tuned to generate paths with different legibility and efficiency characteristics depending on different start and all goal positions. For example, if you wish to exaggerate the path for more legible motions, decrease the attractive coefficient k_p and increase the repulsive coefficient k_n , and adjust the decay coefficient m accordingly. To make the obstacle avoidance effect more significant, consider increasing the vector field strength k_f and adjust the decay coefficient n accordingly. Discussion on manual parameter tuning is presented later in the paper.

TABLE I
PARAMETER TABLE

Definition	Parameter	Value
Start	<i>Start</i>	[3,0]
Goal	<i>Goal</i>	[4,6]
Other Goal	<i>OtherGoal</i>	[2,6]
Obstacle's effective range	s_{obs}	1
Obstacle radius	r_{obs}	0.1
Goal radius (all goals)	r_{goal}	0.25
Other goal effective range	s_{other}	6.08
Attractive coefficient	k_p	$0 \rightarrow 20.0$
Repulsive coefficient	sk_n	$0 \rightarrow 2.0$
Decay coefficient in F_{other}	m	$0 \rightarrow 10.0$
Decay coefficient in F_{ox}, F_{oy}	n	$0 \rightarrow 1.0$
Vector field strength	k_f	$0 \rightarrow 50.0$
Trust Region Threshold [12]	<i>beta</i>	40

B. Legible Motion Without Obstacles

The robot can plan a legible path from the starting point to the real goal (in blue) instead of the other goal (in red) in the case of no obstacle on the map, as shown in Figure 2.

For the Potential Field method [6], the path was a straight line to the goal since there was no repulsive force from any obstacle. For Legible Motion method [12], the path was generated with the trust region threshold value to be 40 (Table I).

Compared to the legible path generated by Dragan et al. [12], our path showed similar exaggerating characteristics of a legible path to the real goal (in blue).

Our results of AULC and TPL metrics in the no obstacle scenario showed that our method generated paths with comparable legibility score to the Legible baseline [12] (5.5% less legible) and significantly more legible than Potential Field baseline [6] (67.6% more legible). Moreover, our method can generate paths that are more efficient than the Legible baseline (8.4% more efficient).

C. Legible Motion With Obstacles

Even with the presence of obstacles, the robot can still plan legible paths to the real goal (in blue) instead of the other goal (in red) while smoothly avoiding obstacles on the way. An illustration is shown in Figure 3.

For the legible path baseline in this case, we also use the method from Dragan et al. [12] by further exaggeration of the path to avoid obstacle. However, the legible baseline from Dragan et al. [12] does not consider real-time obstacle avoidance. Thus, to compare the real-time characteristics, the

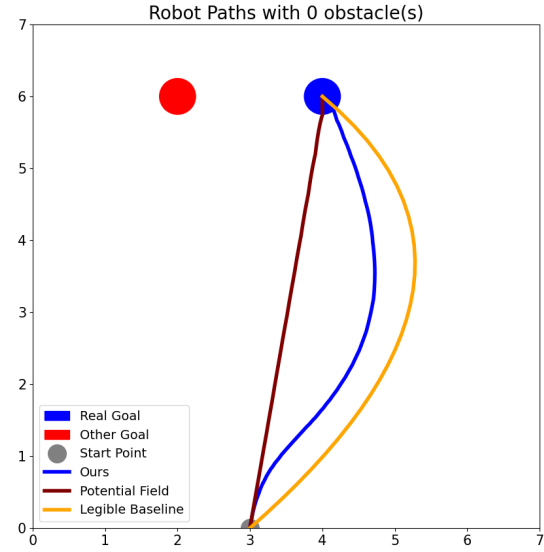


Fig. 2. Legible path to the goal destination (blue) and the repulsive field of the other destination (red). The orange path was the legible baseline from [12], and the maroon path was from the potential field method [6] (maroon).

legible baseline path was only re-planned when the agent was first in contact with the effective radius of the obstacle, hence a slight divergence in the yellow path near the point (4,1) in Figure 3. That re-planned path was generated with the same parameters as the original path, only with a different starting point.

If the obstacle is far away from the original robot path (e.g., the left obstacle in Figure 3), the robot path remained unaffected by the obstacle since the agent was outside that obstacle's effective radius.

Similar to the no obstacle scenario, our results of AULC and TPL metrics in the obstacle scenario showed that our method generated paths with comparable legibility scores to the Legible baseline [12] (28.8% less legible) and significantly more legible than Potential Field baseline [6] (93.6% more legible). Moreover, our method can generate paths that are more efficient than the Legible baseline (10.7% more efficient).

D. Switching Goals

In this scenario, the robot decides to go to another goal at a random point along the path, which could be due to various reasons (e.g., the original goal was occupied). Our method was able to still plan an alternative legible path to the new goal. An illustration is shown in Figure 4.

A goal switch can happen any time, and a new goal can be anywhere on the map. For the sake of easy understanding, we show the simple situation where the positions of the two goals were swapped. For this specific scenario, we only compared the part of the paths from the switching point to

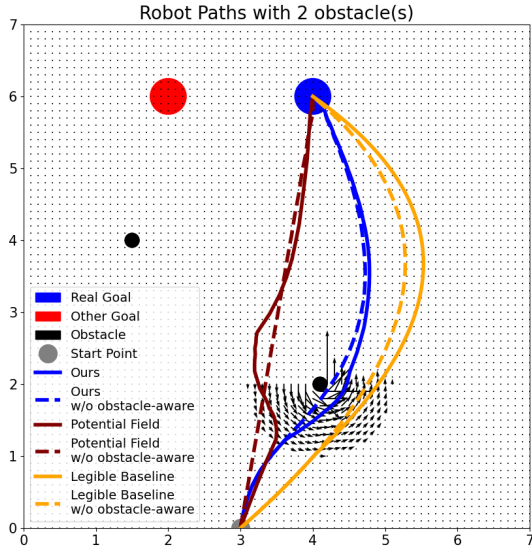


Fig. 3. Legible path from the starting position to the real goal (in blue) instead of the other goal (in red). The robot diverges from its original path (obstacle-aware) if the obstacles are near the original path. The orange path was the legible baseline from [12], and the maroon path was from the potential field method [6]. Dashed paths are from Figure 2 (paths with no obstacle). The white asterisk pattern is an artifact of the rendering.

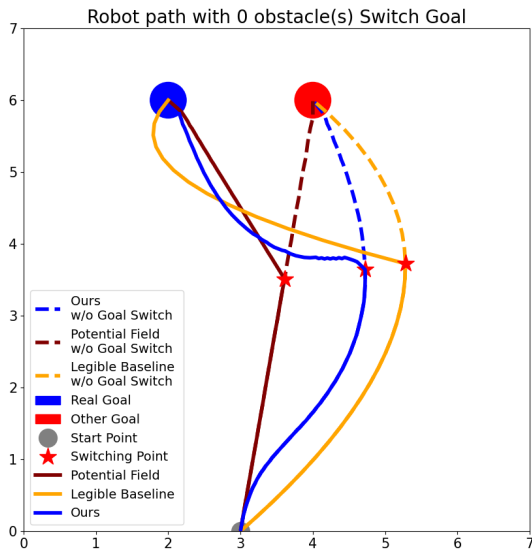


Fig. 4. The robot initially headed for the goal on the right. At a specific point of some distance to the right goal, it decided to switch to the left goal (i.e., realized the right goal is occupied). All the switching points are of equal distance to the right goal. The orange path was the legible baseline from [12], and the maroon path was from the potential field method [6]. All comparisons of legibility and efficiency metrics were performed only on the part of the paths after the switching positions (red star). Dashed paths are from Figure 2 (paths without goal switch).

the left goal. The first part of the path was not measured for this comparison.

For the goal switch case, our results of AULC and TPL metrics in the obstacle scenario shown that our method could generate paths with comparable legibility score to the Legible baseline [12] (8.7% less legible) and more legible than Potential Field baseline [6] (43.5% more legible). Moreover, our method could generate paths that are more efficient than the Legible baseline (18.6% more efficient). Even though we only considered the later part of the path after the switch, the differences in legibility of all methods were still significant compared to the previous scenarios (no obstacle and with obstacle). Thus, our claims still hold for this case.

Moreover, our method has an added advantage of not displaying a sudden change in robot direction. As observed in Figure 4, the heading direction change of the legible baseline (orange path) was very large compared to ours. This implies our method will have more appropriate behavior in real-world robots, as compared to the legible baseline [12].

E. Results Summary

The results of all three scenarios on the two metrics, namely Area Under the Legibility Curve (AULC) and Total Path Length (TPL), are presented in Table II, Figure 5, and Figure 6.

TABLE II

EVALUATION TABLE OF ALL CASES

Case	Metrics	Potential Field	Legible Motion	Ours
No Obstacle	AULC	4.42	7.82	7.41
	TPL	6.09	7.19	6.63
With Obstacle	AULC	5.15	12.84	9.97
	TPL	6.30	7.48	6.76
Goal Switch	AULC	2.55	3.98	3.66
	TPL	2.97	4.60	3.88

From these, our method was consistently able to generate paths on all three scenarios that are of comparable legibility with and more efficient than the Legible Baseline [12]. Moreover, our generated paths were more legible than paths generated by the Potential Field method [6].

VI. DISCUSSION AND FUTURE WORK

A. Optimal Parameters for Motion Generation

Although paths generated by our method have a comparable legibility and shorter length than paths from legible baseline, as well as more legible than paths from potential field method, our set of parameters was tuned manually. Those parameters, such as attractive/repulsive field strengths, obstacle vector field strength, and effective radius, could impact the performance of the path generation process. Future work could use optimization methods to automatically tune and choose the best set of parameters for the best performance based on our proposed metrics.

Moreover, hyper-parameter optimization techniques could be used to achieve the desired results of legibility and efficiency. Grid search [31], while computationally intensive

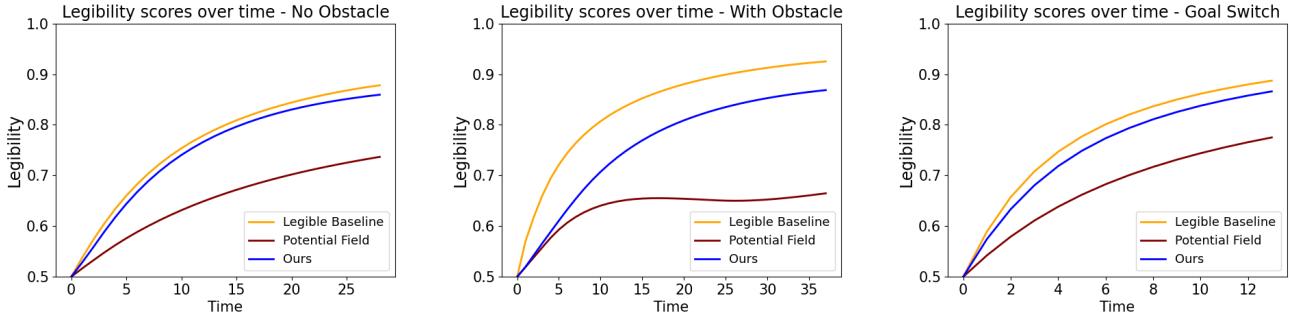


Fig. 5. Legibility scores over time of all three methods in the case of No Obstacle (left), With Obstacle (middle), and Goal Switch (right) on the map: ours (blue), Dragan et al. [12] (orange), and Potential Field [6] (maroon). For the case of Goal Switch, time 0 is the time of the switching position.

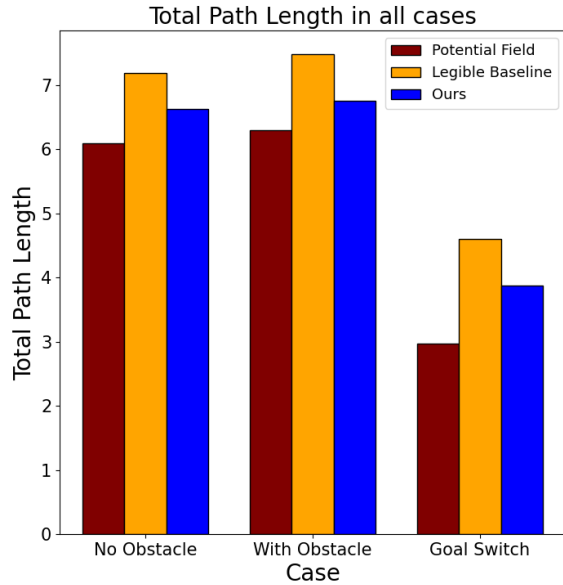


Fig. 6. Total Path Length of all three methods in all cases: ours (blue), Dragan et al. [12] (orange), and Potential Field [6] (maroon).

and limited by the predefined values for each parameters, could be used to optimize parameters, in which the possible ranges of parameter values could be determined by manual searching the first few times (i.e., Table I). Random Search [32] could also be incorporated to optimize parameters due to its simplicity and less computationally intensive. Bayesian optimization [33] is another potential method for tuning parameters, as it has gained popularity in the machine learning community. Due to its ability to consider the previous evaluation results during the parameter tuning process, Bayesian optimization could select the combination that yields the best results, thus being able to choose a good set of parameters in relatively few iterations. Future work could apply these hyper-parameter tuning techniques to generate paths with efficiently shorter path length, while retaining a comparable legibility characteristics.

B. Real-time Characteristics of the Method

Previous works on legible motion planning [1], [12], [8] have not focused on the problem of real-time obstacle avoidance during path generation. They instead concentrated on generating legible paths with known maps. The real-time characteristics of our method was demonstrated through the introduction of the effective radius of the obstacle, in which the robot only plans an alternate path when it travels inside the effective radius of the obstacle. This implies a possible application in the real-world, where the effective radius of the obstacle can be interchanged with the robot's sensor range. I.e., the robot re-plans an alternative path to avoid obstacles only when they appear within sensor range.

Moreover, legible motion planners could consider obstacle avoidance by adding the cost of going near obstacle in their calculation of cost functions. Although our obstacle avoidance method was inspired by vector fields, other types of obstacle avoidance could be modified and integrated for legible motion planning, such as the family of BUG algorithms [34] and their extensions [35]. On the other hand, sampling-based algorithm for obstacle avoidance could also be considered, such as modified strategies from Rapidly-Exploring Random Tree (RRT) [27] and Probabilistic Roadmaps (PRMs) [28].

Finally, our method only considered obstacles appearing on the map, not dynamically moving into the scene, which is not always the case in real-world situations [3], [36] where obstacles have their own dynamics. Our method opens up potential applications to unstructured environments and dynamic obstacles in real-world settings, in which the agent can update the position of the obstacles and adjust its moving direction in every time step. Although not specifically discussed in our paper, our method has potential to scale up and generalize to more complex environments and obstacles. Thus, future work calls for the consideration of obstacles moving in the scene in the generation of legible motions, with obstacles having their own velocities and directions.

C. Human Study

This work focused on developing the planning algorithm for legible motion planning and relied on simulation-friendly metrics, not human ratings. Likewise, other methods considered viewpoints [8] and observers [1] for evaluation, while

this work uses an omniscient observer where everything can be seen from a birds-eye view – a view humans usually do not have access to. Thus, a comparison to state-of-the-art methods as baselines using one or more human studies in real-world scenarios is a direction for future work.

VII. CONCLUSION

By combining the advantages of the Potential Field method and the Vector Field method for obstacle-aware path planning, we were able to generate paths that are similarly legible with and of shorter path length than paths generated by previous legible motion planning work. Moreover, our method could produce legible paths that are significantly more legible than ones generated by traditional potential field method. Those differences demonstrated using evaluation metrics, Area Under the Legibility Curve and Total Path Length, in human-centered scenarios where legibility is valued. Our method also demonstrated more human-appropriate handling of newly detected obstacles and goal changes.

REFERENCES

- [1] A. V. Taylor, E. Mamantov, and H. Admoni, "Observer-aware legibility for social navigation," in *2022 31st IEEE International Conference on Robot and Human Interactive Communication (RO-MAN)*. IEEE, 2022, pp. 1115–1122.
- [2] A. H. Quispe, H. B. Amor, and M. Stilman, "Handover planning for every occasion," in *2014 IEEE-RAS International Conference on Humanoid Robots*. IEEE, 2014, pp. 431–436.
- [3] J. Hardy and M. Campbell, "Contingency planning over probabilistic obstacle predictions for autonomous road vehicles," *IEEE Transactions on Robotics*, vol. 29, no. 4, pp. 913–929, 2013.
- [4] Y. Lin and S. Saripalli, "Sampling-based path planning for uav collision avoidance," *IEEE Transactions on Intelligent Transportation Systems*, vol. 18, no. 11, pp. 3179–3192, 2017.
- [5] A. D. Dragan, K. C. Lee, and S. S. Srinivasa, "Legibility and predictability of robot motion," in *2013 8th ACM/IEEE International Conference on Human-Robot Interaction (HRI)*. IEEE, 2013, pp. 301–308.
- [6] Y. K. Hwang, N. Ahuja *et al.*, "A potential field approach to path planning," *IEEE transactions on robotics and automation*, vol. 8, no. 1, pp. 23–32, 1992.
- [7] D. Panagou, "Motion planning and collision avoidance using navigation vector fields," in *2014 IEEE International Conference on Robotics and Automation (ICRA)*. IEEE, 2014, pp. 2513–2518.
- [8] S. Nikolaidis, A. Dragan, and S. Srinivasa, "Viewpoint-based legibility optimization," in *ACM/IEEE International Conference on Human-Robot Interaction*, vol. 2016, 2016, pp. 271–278.
- [9] M. Huber, M. Rickert, A. Knoll, T. Brandt, and S. Glasauer, "Human-robot interaction in handing-over tasks," in *RO-MAN 2008-the 17th IEEE international symposium on robot and human interactive communication*. IEEE, 2008, pp. 107–112.
- [10] S. Parastegari, B. Abbasi, E. Noohi, and M. Zefran, "Modeling human reaching phase in human-human object handover with application in robot-human handover," in *2017 IEEE/RSJ International Conference on Intelligent Robots and Systems (IROS)*. IEEE, 2017, pp. 3597–3602.
- [11] M. Zheng, A. Moon, E. A. Croft, and M. Q.-H. Meng, "Impacts of robot head gaze on robot-to-human handovers," *International Journal of Social Robotics*, vol. 7, pp. 783–798, 2015.
- [12] A. Dragan and S. Srinivasa, "Generating legible motion," 2013.
- [13] R. M. Holladay, A. D. Dragan, and S. S. Srinivasa, "Legible robot pointing," in *The 23rd IEEE International Symposium on robot and human interactive communication*. IEEE, 2014, pp. 217–223.
- [14] C. Bodden, D. Rakita, B. Mutlu, and M. Gleicher, "Evaluating intent-expressive robot arm motion," in *2016 25th IEEE International Symposium on Robot and Human Interactive Communication (RO-MAN)*. IEEE, 2016, pp. 658–663.
- [15] J. Reinhardt and K. Bengler, "Design of a hesitant movement gesture for mobile robots," *Plos one*, vol. 16, no. 3, p. e0249081, 2021.
- [16] J. Sun, J. Tang, and S. Lao, "Collision avoidance for cooperative uavs with optimized artificial potential field algorithm," *IEEE Access*, vol. 5, pp. 18 382–18 390, 2017.
- [17] J. P. Wilhelm and G. Clem, "Vector field uav guidance for path following and obstacle avoidance with minimal deviation," *Journal of Guidance, Control, and Dynamics*, vol. 42, no. 8, pp. 1848–1856, 2019.
- [18] H. Chen, K. Chang, and C. S. Agate, "Uav path planning with tangent-plus-lyapunov vector field guidance and obstacle avoidance," *IEEE Transactions on Aerospace and Electronic Systems*, vol. 49, no. 2, pp. 840–856, 2013.
- [19] S. M. H. Rostami, A. K. Sangaiah, J. Wang, and X. Liu, "Obstacle avoidance of mobile robots using modified artificial potential field algorithm," *EURASIP Journal on Wireless Communications and Networking*, vol. 2019, no. 1, pp. 1–19, 2019.
- [20] P. E. Hart, N. J. Nilsson, and B. Raphael, "A formal basis for the heuristic determination of minimum cost paths," *IEEE transactions on Systems Science and Cybernetics*, vol. 4, no. 2, pp. 100–107, 1968.
- [21] M. Noto and H. Sato, "A method for the shortest path search by extended dijkstra algorithm," in *Smc 2000 conference proceedings. 2000 ieee international conference on systems, man and cybernetics.'cybernetics evolving to systems, humans, organizations, and their complex interactions'(cat. no. 0, vol. 3)*. IEEE, 2000, pp. 2316–2320.
- [22] C. Hernández and P. Meseguer, "Lrt α *(k)," in *Proceedings of the 19th international joint conference on Artificial intelligence*, 2005, pp. 1238–1243.
- [23] S. Koenig and M. Likhachev, "D* lite," in *Eighteenth national conference on Artificial intelligence*, 2002, pp. 476–483.
- [24] J. Ng and T. Bräunl, "Performance comparison of bug navigation algorithms," *Journal of Intelligent and Robotic Systems*, vol. 50, pp. 73–84, 2007.
- [25] A. Yufka and O. Parlaktuna, "Performance comparison of bug algorithms for mobile robots," in *Proceedings of the 5th international advanced technologies symposium, Karabuk, Turkey*, 2009, pp. 13–15.
- [26] S. M. LaValle and J. J. Kuffner, "Rapidly-exploring random trees: Progress and prospects: Steven m. lavalle, iowa state university, a james j. kuffner, jr., university of tokyo, tokyo, japan," *Algorithmic and computational robotics*, pp. 303–307, 2001.
- [27] S. Karaman, M. R. Walter, A. Perez, E. Frazzoli, and S. Teller, "Anytime motion planning using the rrt," in *2011 IEEE international conference on robotics and automation*. IEEE, 2011, pp. 1478–1483.
- [28] L. E. Kavraki, P. Svestka, J.-C. Latombe, and M. H. Overmars, "Probabilistic roadmaps for path planning in high-dimensional configuration spaces," *IEEE transactions on Robotics and Automation*, vol. 12, no. 4, pp. 566–580, 1996.
- [29] J. Myerson, L. Green, and M. Warusawitharana, "Area under the curve as a measure of discounting," *Journal of the experimental analysis of behavior*, vol. 76, no. 2, pp. 235–243, 2001.
- [30] E. McQuillin, N. Churamani, and H. Gunes, "Learning socially appropriate robo-waiter behaviours through real-time user feedback," in *2022 17th ACM/IEEE International Conference on Human-Robot Interaction (HRI)*. IEEE, 2022, pp. 541–550.
- [31] P. Liashchynskyi and P. Liashchynskyi, "Grid search, random search, genetic algorithm: a big comparison for nas," *arXiv preprint arXiv:1912.06059*, 2019.
- [32] R. G. Mantovani, A. L. Rossi, J. Vanschoren, B. Bischi, and A. C. De Carvalho, "Effectiveness of random search in svm hyper-parameter tuning," in *2015 international joint conference on neural networks (IJCNN)*. Ieee, 2015, pp. 1–8.
- [33] J. Wu, X.-Y. Chen, H. Zhang, L.-D. Xiong, H. Lei, and S.-H. Deng, "Hyperparameter optimization for machine learning models based on bayesian optimization," *Journal of Electronic Science and Technology*, vol. 17, no. 1, pp. 26–40, 2019.
- [34] K. N. McGuire, G. C. de Croon, and K. Tuyls, "A comparative study of bug algorithms for robot navigation," *Robotics and Autonomous Systems*, vol. 121, p. 103261, 2019.
- [35] K. Taylor and S. M. LaValle, "I-bug: An intensity-based bug algorithm," in *2009 IEEE International Conference on Robotics and Automation*. IEEE, 2009, pp. 3981–3986.
- [36] A. Cherubini, F. Spindler, and F. Chaumette, "Autonomous visual navigation and laser-based moving obstacle avoidance," *IEEE Transactions on Intelligent Transportation Systems*, vol. 15, no. 5, pp. 2101–2110, 2014.